Direct Determination of the Electron-Phonon Coupling Matrix Element in a Correlated System

Huajun Qin,[1] Junren Shi,[2,1] Yanwei Cao,[1] Kehui Wu,[1] Jiandi Zhang,[3] E. W. Plummer,[3] J. Wen,[4] Z. J. Xu,[4] G. D. Gu,[4] and Jiandong Guo[1]

[1]*Beijing National Laboratory for Condensed-Matter Physics and Institute of Physics, Chinese Academy of Sciences, Beijing 100190, China*

[2]*International Center for Quantum Materials, Peking University, Beijing 100871, China*

[3]*Department of Physics and Astronomy, Louisiana State University, Baton Rouge, Louisiana 70808, USA*

[4]*Brookhaven National Laboratory, Upton, New York 11973, USA*

(Received 23 April 2010; published 15 December 2010)

High-resolution electron energy loss spectroscopy measurements have been carried out on an optimally doped cuprate $Bi_2Sr_2CaCu_2O_{8+\delta}$. The momentum-dependent energy and linewidth of an A_1 optical phonon were obtained. Based on these data as well as detailed knowledge of the electronic structure, we developed a scheme to determine the electron-phonon coupling (EPC) matrix element related to a specific phonon mode. Such an approach is general and applicable to elucidating the full structure of EPC in a system with anisotropic electronic structure.

DOI: 10.1103/PhysRevLett.105.256402 PACS numbers: 71.27.+a, 71.38.−k, 74.72.−h, 79.20.Uv

The interaction between electrons and various collective excitations (bosons) is the central ingredient for understanding many of the novel physical properties in condensed-matter systems [1–3]. For simple systems with isotropic electronic structures, such an interaction [electron-boson coupling (EBC)] can be characterized by the Eliashberg spectral function $\alpha^2F(\omega)$ [4], which describes the energy of the bosonic modes involved as well as their coupling strengths. Thus it is important to directly determine the Eliashberg function. For instance, in Pb, it played a crucial role in establishing the BCS theory of superconductivity [5]. Experimentally, there exist several techniques for determining the Eliashberg function, such as the McMillan-Rowell inversion method applied to the tunneling data of the conventional superconductors [5,6], and more recently, the maximum entropy method in analyzing the quasiparticle dispersion kink observed in angle-resolved photoemission spectroscopy (ARPES) measurements [7–9]. These approaches attempt to elucidate the EBC by probing its effects on the electrons. On the other hand, effects of the EBC on bosonic modes are not commonly investigated.

For more complex systems, neither the isotropic $\alpha^2F(\omega)$ nor the anisotropic $\alpha^2F(\omega, \hat{\boldsymbol{k}})$ determined from ARPES is sufficient for fully characterizing EBC. A notable example is the high-T_c cuprate, which has highly anisotropic electronic structure and unconventional $d_{x^2-y^2}$ superconductivity. By probing the electrons alone, one can at best determine $\alpha^2F(\omega, \hat{\boldsymbol{k}})$ with dependence on the direction $\hat{\boldsymbol{k}}$ alone using ARPES and the aforementioned maximum entropy method analysis [10]. However, unlike the case of the conventional s-wave superconductors, the so-determined Eliashberg function cannot be directly related to the strength of the unconventional $d_{x^2-y^2}$ pairing. This is because the Eliashberg function and the $d_{x^2-y^2}$ pairing strength belong to different symmetries [11]. For these systems, it is necessary to resolve the full structure of the EBC [i.e., the matrix element $g(\boldsymbol{k}, \boldsymbol{k}')$], which characterizes the probability amplitude for the electron transition from $\boldsymbol{k}$ to $\boldsymbol{k}'$ induced by interaction with bosons [12,13]. Because measurements such as ARPES only contain information about the electron final state $\boldsymbol{k}'$, with the contributions from the different initial states $\boldsymbol{k}$ integrated, it is in general impossible to determine the full structure of $g(\boldsymbol{k}, \boldsymbol{k}')$ by probing electrons alone. Manifestation of the EBC on the bosonic modes also needs to be probed.

In this Letter, we developed a method to resolve the full structure of EBC by probing the bosonic modes, in this case phonons, with high-resolution electron energy loss spectroscopy (HREELS) [14] for the phonons and by using existing ARPES data for the electrons. The momentum-dependent linewidth, as well as the dispersion of an A_1 optical phonon, were measured as a function of the direction relative to the crystalline orientation. The initial and final states involved in the coupling and the corresponding strength are simultaneously determined. The developed scheme is general and particularly applicable to many systems with anisotropic electronic structures.

We used the high-T_c cuprate $Bi_2Sr_2CaCu_2O_{8+\delta}$ (referred to as BSCCO in the following) [15,16] as a test system, whose electronic band structure, Fermi surface, and surface properties have been well characterized [17]. Many experiments have revealed a signature of EBC. ARPES studies showed the electron self-energy renormalization in the form of kinks in the dispersion at energy scales of ~70 meV below the Fermi energy in the nodal region [18–21] and ~40 meV near the antinodal region [13,22]. Direct measurements of phonon spectra have been carried out with Raman spectroscopy [23], infrared spectroscopy [24], HREELS [25], inelastic neutron scattering

[26], and inelastic x-ray scattering [27] for BSCCO and other high-T_c cuprates. However, a systematic study of the momentum-dependent phonon renormalization, which is important for elucidating the details of EBC, is still missing.

The experiments were carried out in a commercial system containing variable-temperature scanning tunneling microscope (STM) and HREELS (LK-5000). The base pressure was better than 1×10^{-10} mbar. The superconducting property of the optimally doped BSCCO single crystal was carefully characterized with a transition temperature at $T_c = 91$ K. The sample was cleaved *in situ* in vacuum. Atomically flat surface was obtained exposing the Bi-O plane with the (1×5) superstructure as characterized with STM and low-energy electron diffraction, which also indicates the relative angle of the crystalline orientation to the measurement geometry. The HREELS measurements were taken with an electron incident angle of 65°, and excitation energy ranging from 3.5 to 50 eV. All the observed spectral features showed no excitation energy dependence. Therefore we employed an excitation energy of 50 eV that offered a wide momentum transfer range. The HREELS sample stage was coupled to a constant-flow liquid helium cryostat, and the measurements were taken at different temperatures ranging from 60 to 300 K, across the superconducting T_c.

Angle-resolved HREELS of the optimally doped BSCCO sample was measured along different directions relative to the crystalline orientation, as shown in Fig. 1. At the Brillouin zone (BZ) center (the in-plane momentum transfer $\boldsymbol{q} = 0$), two main features are resolved near 50 (F_1) and 80 meV (F_2), respectively. The feature F_1 corresponds to the out-of-plane vibration of oxygen atoms in the Bi-O plane [23–25], with two shoulders at both sides with energies of ~41 and ~62 meV that were reported earlier [25]. The feature F_2, with a major focus in the following, appears as a main peak at ~80 meV with a broad tail extending to high energies. The vibration along the c axis of the apical oxygen atoms in the Cu-O semioctahedra is responsible for the main peak [23–25], while the high-energy tail might be related to the imperfections. Also, considering the selection rule of HREELS, we were able to rule out other energy loss mechanisms that fall into this energy range, such as the phonons of the in-plane breathing modes of oxygen in the Cu-O_2 plane because they are not dipole active along the surface normal and therefore undetectable by HREELS at the BZ center. Along any measurement direction, we detected no obvious temperature dependence across superconducting T_c.

As shown in Fig. 1(c), the most prominent characteristic of the momentum-resolved HREELS is observed along the nodal direction ($\varphi = 45°$) where dispersion of the 80-meV feature F_2 softens significantly from the BZ center toward the boundary (half of the BZ length $\pi/a_0 = 0.82$ Å^{-1}). The momentum-dependent phonon energy ($\Omega_{\boldsymbol{q}}$) and the FWHM [$\Gamma(\boldsymbol{q})$] along different directions relative to the crystalline orientation are shown in Fig. 2. An abrupt phonon softening occurs (from 81 to 74 meV) with an onset at $q_{\parallel} \approx 0.45$ Å^{-1}. With the same onset as indicated by the arrows in Fig. 2, $\Gamma(\boldsymbol{q})$ increases suddenly from

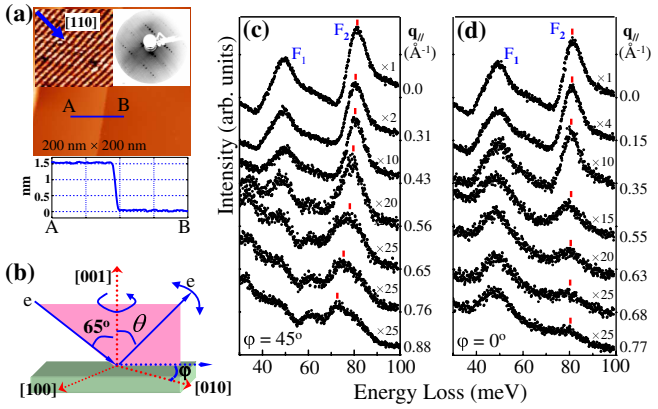

FIG. 1 (color online). (a) STM image of the cleaved BSCCO surface. The left inset shows the 1×5 superstructure with the "×5" direction aligning to [110] orientation. The right inset shows the low-energy electron diffraction patterns taken with beam energy of 61 eV at room temperature. The line profile along AB is displayed in the lower panel, which indicates a step of 1.5 nm corresponding to the interspacing between two cleavable BiO planes. (b) Schematic drawing of the scattering geometry for the angle-resolved HREELS measurements. (c),(d) The HREELS spectra measured with $\varphi = 45°$ and 0°, respectively, with an excitation energy of 50 eV at 60 K. The bars (red) are guides to the eye for the phonon energy shift.

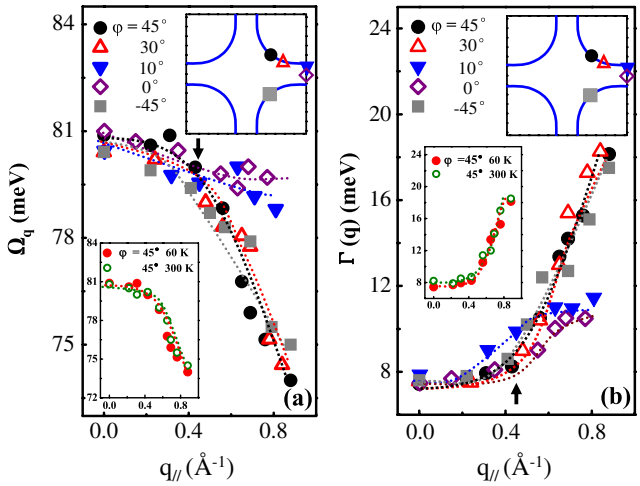

FIG. 2 (color online). (a) $\Omega_{\boldsymbol{q}}$ and (b) $\Gamma(\boldsymbol{q})$ of the apical oxygen phonon at 60 K. The upper insets illustrate the azimuth angles of $q_{\parallel}$ with corresponding symbols in k space relative to the Fermi surface, while the lower insets show the data taken at different temperatures across superconducting T_c. The dotted lines are guides to the eye. Because of the existence of the (1×5) superstructure, there are two irreducible nodal directions ($\varphi = \pm 45°$). Our measurements show identical momentum dependence along both directions.

8 meV at $q_{\parallel} \sim 0.45$ Å^{-1} to 18 meV at $q_{\parallel} \sim 0.8$ Å^{-1}. This behavior is a signature of strong electron-phonon coupling (EPC).

Both Ω_q and $\Gamma(q)$ show a dramatic dependence on the crystalline orientation φ. As φ decreases from 45° (the nodal region), the anomalous behavior persists until φ gets close to the antinodal region ($\varphi \leq 10°$), when neither the energy nor the linewidth shows a prominent momentum dependence at temperatures above or below T_c [also see Fig. 1(d)]. Therefore, Ω_q and $\Gamma(q)$ measured with different φ values can be divided into two groups, respectively. Near the nodal region, Ω_q decreases and $\Gamma(q)$ increases suddenly with the same onset. In contrast, near the antinodal region, $\Gamma(q)$ increases slowly by less than 3 meV while Ω_q is almost momentum independent. It is worth noting that the HREELS spectra show a weak shoulder at ~81 meV [see high-$q_{\parallel}$ spectra in Fig. 1(c)], which can be deconvoluted from the main feature in all spectra by fitting with two Fano functions. The deconvolution indicates that this high-energy shoulder is weak and completely $q_{\parallel}$ independent, consistent with the characteristics of the vibrations connected to the distorted or nonideal structure of the sample or to the extra oxygen atoms in the Bi-O layers [23,28]. Furthermore, the influence of the shoulder, as well as that of the electron-hole pair excitations at high-energy side of F_2 on the analyses of $\Gamma(q)$, can be eliminated by measuring $\Gamma(q)$ from the left side of the peak only.

The dramatic behavior observed in the phonon spectra is undoubtedly related to the electronic structure and specifically to EPC. The following is a formalism that allows us to decouple the anisotropic electron properties from the EPC matrix element. In general, the momentum-dependent phonon broadening $\Gamma_{\mathrm{EPC}}(q)$ induced by EPC can be written as [4]

$$\Gamma_{\mathrm{EPC}}(q) = -2|g(q)|^2 \,\mathrm{Im}[\chi(q, \Omega_q)], \tag{1}$$

where $\chi(q, \Omega_q)$ is the Lindhard response function and $|g(q)|^2$ is the EPC matrix element in a surface Brillouin zone. We have assumed the EPC matrix element to be $g(k, k') = g(k' - k) \equiv g(q)$, which is a good approximation for the particular out-of-plane apical oxygen phonon mode. The imaginary part of $\chi(q, \Omega_q)$ is given by

$$\mathrm{Im}[\chi(q, \omega)] = \int_{\mathrm{BZ}} \frac{dk}{2\pi} [f_{k+q} - f_k] \delta(\hbar\omega + \epsilon_k - \epsilon_{k+q}), \tag{2}$$

where $f_k \equiv f(\epsilon_k)$ is the Fermi distribution function and ϵ_k is the energy dispersion of the quasielectrons. The quasiparticle dispersion ϵ_k of BSCCO has been measured previously (ARPES) and fitted in a tight-binding phenomenological model [17,29]. $\mathrm{Im}[\chi(q, \Omega_q)]$ can then be calculated numerically, as shown in Fig. 3(a), which displays rather complicated features originating from the highly anisotropic electronic structure.

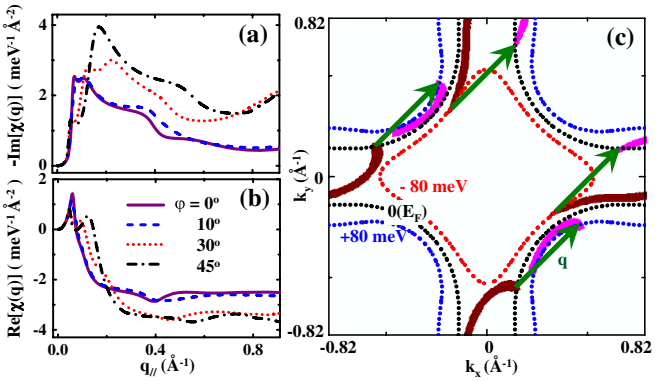

FIG. 3 (color online). (a),(b) The imaginary and real parts of $\chi(q, \Omega_q)$ calculated with Eqs. (2) and (6), respectively, at 60 K for different φ. (c) The energy contour plot (dotted lines) of the quasiparticle band near E_F of BSCCO. The initial states contributing to the EPC-induced broadening for $q_{\parallel} \sim 0.47$ Å^{-1} at $\varphi = 45°$ can be determined by superimposing the density plot of the integrating function in Eq. (2) [dark (brown) areas] onto (c). Connecting by q (indicated by the arrows), the final states [light (pink) areas] correspond to an energy gain that equals $\hbar\Omega_q$.

The experimentally observed $\Gamma(q)$ also include a momentum-independent background Γ_0, which mostly originates from the surface roughness of the cleaved sample and the instrumentation broadening:

$$\Gamma_{\mathrm{exp}}(q) = \Gamma_0 + \Gamma_{\mathrm{EPC}}(q). \tag{3}$$

We estimate such a background using the value of the experimental data near $q = 0$: $\Gamma_0 = \Gamma_{\mathrm{exp}}(q \to 0)$, since there should have been no EPC-induced broadening at $q = 0$. With the background subtracted, the EPC matrix element can then be determined straightforwardly by $|g(q)|^2 = -\Gamma_{\mathrm{EPC}}(q)/2\,\mathrm{Im}[\chi(q, \Omega_q)]$. We note that the determined $|g(q)|^2$ does not show a strong dependence on the measurement direction φ, indicating that the dramatically different behaviors for nodal and antinodal directions observed in the phonon linewidth are mainly due to the anisotropy in the electronic structure.

The determined EPC matrix element $|g(q)|^2$ is shown in Fig. 4(a). Using the least-squares method, the data can be well fitted by

$$|g_q|^2 = \{(2a + b) - a[\cos(q_x a_0) + \cos(q_y a_0)] - b\cos(q_x a_0)\cos(q_y a_0)\}^2, \tag{4}$$

which is consistent with an A_1 phonon mode that couples to electrons in the lattice with C_{4v} symmetry. Here a and b are constants, representing the coupling strength between an atom displacement and its nearest and next-nearest neighboring sites, respectively.

Only the electron transition satisfying both energy and momentum conservations, i.e., $k' - k = q$ and $\epsilon_{k'} - \epsilon_k = \hbar\Omega_q$, contributes to the EPC-induced broadening. This imposes a stringent constraint on the possible initial

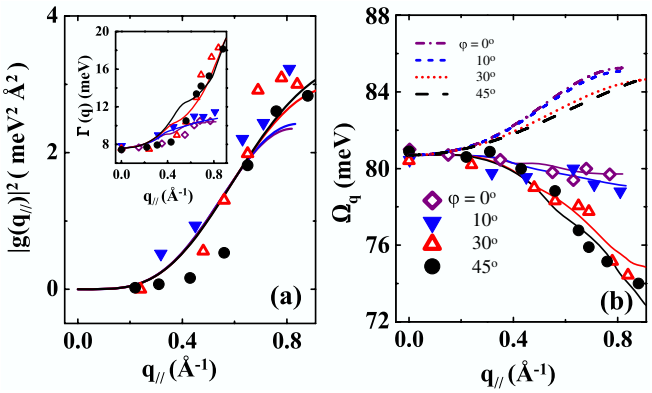

FIG. 4 (color online). (a) $|g_q|^2$ determined by Eqs. (1)–(3) and the fitting (solid lines) to Eq. (4) with $a = 0.47$ meV Å and $b = 0.29$ meV Å. The inset shows the measured $\Gamma(\boldsymbol{q})$ as well as the data calculated with $|g_q|^2$ for different φ. (b) Measured $\Omega(\boldsymbol{q})$ with data calculated with Eq. (5). Here we assume a bare phonon dispersion $\Omega^{\text{bare}} = 83.5 - 1.16[\cos(q_x a_0) + \cos(q_y a_0)] - 1.11\cos(q_x a_0)\cos(q_y a_0) + 0.32[\cos(2q_x a_0) + \cos(2q_y a_0)]$(meV), as plotted in broken lines.

and final states of electron for a given phonon momentum $\boldsymbol{q}$. Therefore, the determined $|g(\boldsymbol{q})|^2$ should be considered as a subset of the more general $|g(\boldsymbol{k}, \boldsymbol{k}')|^2$. Figure 3(c) depicts the electronic excitations near E_F with a fixed momentum transfer $\boldsymbol{q}$ contributing to the EPC-induced broadening.

To further test our analysis, we calculate the phonon softening induced by EPC [4]:

$$\Omega(\boldsymbol{q}) = \sqrt{\Omega^{\text{bare}}(\boldsymbol{q})^2 + 2\Omega^{\text{bare}}(\boldsymbol{q})|g_{\boldsymbol{q}}|^2 \text{Re}[\chi(\boldsymbol{q}, \Omega_{\boldsymbol{q}})]}, \quad (5)$$

$$\text{Re}\,[\chi(\boldsymbol{q}, \omega)] = 2\int_{\text{BZ}} \frac{d\boldsymbol{k}}{(2\pi)^2} \frac{f_{\boldsymbol{k}} - f_{\boldsymbol{k}+\boldsymbol{q}}}{\epsilon_{\boldsymbol{k}} - \epsilon_{\boldsymbol{k}+\boldsymbol{q}} + \hbar\omega}, \quad (6)$$

where $\text{Re}[\chi(\boldsymbol{q}, \omega)]$ is the real part of the Lindhard response function, as plotted in Fig. 3(b), and $\Omega^{\text{bare}}(\boldsymbol{q})$ is the fictitious bare phonon dispersion in the absence of EPC. Figure 4(b) shows the fittings to the experimental data of the phonon dispersion, as well as the assumed $\Omega^{\text{bare}}(\boldsymbol{q})$. It is important to note that, in contrast with $\Omega(\boldsymbol{q})$, $\Omega^{\text{bare}}(\boldsymbol{q})$ are nearly isotropic, indicating that the large anisotropy of the phonon softening observed in the experiment originates from EPC.

In conclusion, we demonstrate that the EPC matrix element $|g(\boldsymbol{q})|^2$ for a specific phonon mode can be determined directly by measuring the phonon structure with HREELS, on the basis of a detailed knowledge of the electronic structure of the system. Such an approach is completely general and could be applicable for other complex systems with highly anisotropic electronic structures. Our study also highlights the necessity of probing bosons for revealing the full structure of EBC in these complex systems.

This work is supported by Chinese NSF-10704084, Chinese MOST (2006CB921300 and 2007CB936800), and NSF (DMR-0346826, DMR-0451163, DMS & E). J. Z. and J. G. gratefully acknowledge the support of K. C. Wong Education Foundation, Hong Kong.

[1] J. P. Carbotte, Rev. Mod. Phys. **62**, 1027 (1990).
[2] M. L. Kulić, Phys. Rep. **338**, 1 (2000).
[3] O. Gunnarsson and O. Rösch, J. Phys. Condens. Matter **20**, 043201 (2008).
[4] Göran Grimvall, *The Electron-Phonon Interaction In Metals* (North-Holland, Amsterdam, 1981), p. 196.
[5] J. M. Rowell *et al.*, Phys. Rev. Lett. **10**, 334 (1963); D. J. Scalapino *et al.*, Phys. Rev. **148**, 263 (1966).
[6] W. McMillan and J. Rowell, in *Superconductivity*, edited by R. D. Park (Marcel Dekker, New York, 1969), Vol 1.
[7] J. R. Shi *et al.*, Phys. Rev. Lett. **92**, 186401 (2004).
[8] X. J. Zhou *et al.*, Phys. Rev. Lett. **95**, 117001 (2005).
[9] W. Meevasana *et al.*, Phys. Rev. Lett. **96**, 157003 (2006).
[10] T. Chien *et al.*, Phys. Rev. B **80**, 241416(R) (2009).
[11] N. Bulut and D. J. Scalapino, Phys. Rev. B **54**, 14 971 (1996).
[12] T. Devereaux *et al.*, Phys. Rev. Lett. **93**, 117004 (2004).
[13] T. Cuk *et al.*, Phys. Rev. Lett. **93**, 117003 (2004).
[14] H. Ibach and D. L. Mills, *Electron Energy Loss Spectroscopy and Surface Vibrations* (Academic, New York, 1982).
[15] J. C. Campuzano *et al.*, Phys. Rev. Lett. **83**, 3709 (1999).
[16] T. Cuk *et al.*, Phys. Status Solidi B **242**, 11 (2005).
[17] A. Damascelli *et al.*, Rev. Mod. Phys. **75**, 473 (2003).
[18] A. Lanzara *et al.*, Nature (London) **412**, 510 (2001).
[19] P. V. Bogdanov *et al.*, Phys. Rev. Lett. **85**, 2581 (2000).
[20] P. D. Johnson *et al.*, Phys. Rev. Lett. **87**, 177007 (2001).
[21] J. D. Koralek *et al.*, Phys. Rev. Lett. **96**, 017005 (2006).
[22] A. D. Gromko *et al.*, Phys. Rev. B **68**, 174520 (2003).
[23] M. Kakihana *et al.*, Phys. Rev. B **53**, 11 796 (1996).
[24] N. N. Kovaleva *et al.*, Phys. Rev. B **69**, 054511 (2004).
[25] R. Phelps *et al.*, Phys. Rev. B **48**, 12 936 (1993).
[26] L. Pintschovius *et al.*, Phys. Status Solidi B **242**, 30 (2005).
[27] J. Graf *et al.*, Phys. Rev. Lett. **100**, 227002 (2008).
[28] M. Osada *et al.*, Phys. Rev. B **56**, 2847 (1997).
[29] M. R. Norman *et al.*, Phys. Rev. B **52**, 615 (1995).